





Article

Polymeric Surfactant P84/Polyoxometalate α -PW₁₂O₄₀^{3−} — A Model System to Investigate the Interplay between Chaotropic and Hydrophobic Effects

Philipp Schmid ^{1,2} , Xaver Graß ¹, Pratap Bahadur ³, Isabelle Grillo ^{4,†}, Olivier Diat ² , Arno Pfitzner ¹ 
and Pierre Bauduin ^{2,*} 

- ¹ Institute of Inorganic Chemistry, University of Regensburg, Universitätsstraße 31, 93053 Regensburg, Germany; philipp.schmid@chemie.uni-regensburg.de (P.S.); xaver.grass@stud.uni-regensburg.de (X.G.); arno.pfitzner@chemie.uni-regensburg.de (A.P.)
² ICSM, Univ Montpellier, CNRS, ENSCM, CEA, 30207 Bagnols sur Cèze, France; olivier.diat@cea.fr
³ Department of Chemistry, Veer Narmad South Gujarat University, Surat 395 007, India; pbahadur2002@yahoo.com
⁴ Institut Laue-Langevin (ILL), 71 Avenue des Martyrs CS 20156, CEDEX 9, 38042 Grenoble, France; grillo@ill.fr
* Correspondence: pierre.bauduin@cea.fr
† In memory of Dr. Isabelle Grillo.

Abstract: Low charge density nanometric ions were recently shown to bind strongly to neutral hydrated matter in aqueous solution. This phenomenon, called the (super-)chaotropic effect, arises from the partial dehydration of both the nano-ion and the solute, leading to a significant gain in enthalpy. Here, we investigate the chaotropic effect of the polyoxometalate α -PW₁₂O₄₀^{3−} on the triblock copolymer P84: (EO)₁₉(PO)₄₃(EO)₁₉ with (EO)₁₉ the polyethoxylated and (PO)₄₃ the polypropoxylated chains. The combination of phase diagrams, spectroscopic (nuclear magnetic resonance) and scattering (small angle neutron/X-ray scattering) techniques revealed that: (i) below the micellization temperature of P84, PW₁₂O₄₀^{3−} exclusively binds to the propylene oxide moiety of P84 unimers; and (ii) above the micellization temperature, PW₁₂O₄₀^{3−} mostly adsorbs on the ethylene oxide micellar corona. The preferential binding of the PW₁₂O₄₀^{3−} to the PPO chain over the PEO chains suggests that the binding is driven by the chaotropic effect and is reinforced by the hydrophobic effect. At higher temperatures, copolymer micellization leads to the displacement of PW₁₂O₄₀^{3−} from the PPO chain to the PEO chains. This study deepens our understanding of the subtle interplay between the chaotropic and hydrophobic effects in complex salt-organic matter solutions.

Keywords: chaotropic effect; hydrophobic effect; polyoxometalates; polymeric surfactants; small angle scattering; salt effects



Citation: Schmid, P.; Graß, X.; Bahadur, P.; Grillo, I.; Diat, O.; Pfitzner, A.; Bauduin, P. Polymeric Surfactant P84/Polyoxometalate α -PW₁₂O₄₀^{3−}—A Model System to Investigate the Interplay between Chaotropic and Hydrophobic Effects. *Colloids Interfaces* **2022**, *6*, 16. <https://doi.org/10.3390/colloids6010016>

Academic Editor: Wuge Briscoe

Received: 26 January 2022

Accepted: 23 February 2022

Published: 1 March 2022

Publisher's Note: MDPI stays neutral with regard to jurisdictional claims in published maps and institutional affiliations.



Copyright: © 2022 by the authors. Licensee MDPI, Basel, Switzerland. This article is an open access article distributed under the terms and conditions of the Creative Commons Attribution (CC BY) license (<https://creativecommons.org/licenses/by/4.0/>).

1. Introduction

Polyoxometalates (POMs) have been the object of growing interest in chemistry due to their outstanding properties, e.g., their (photo-)catalytic activity [1–3], applications in medicine [4–6], etc. [7,8]. Currently, the solution behavior of POMs in aqueous media has attracted much attention in the literature [9,10]. It was demonstrated that POMs with a low charge density, such as phosphotungstate (α -PW₁₂O₄₀^{3−}, PW) (see Figure 1a), bind strongly and noncovalently to hydrated surfaces of nonionic micelles in aqueous solution [11]. This phenomenon—known as the (super-)chaotropic effect—has been described as a water-mediated effect: the hydration shells of both the POM and (surface) moieties are partially stripped during binding. The superchaotropic effect is an enthalpy-driven process which has been discussed as an extension of the well-known Hofmeister series observed for smaller classical chaotropic ions, such as I[−] or SCN[−], in many physico-chemical and biological phenomena [12,13]. The association constants of superchaotropic POMs and other nano-ions (NIs), e.g., ionic boron clusters, with neutral organic solutes/surfaces are

typically around three orders of magnitude stronger than those of common chaotropic ions. For this reason low charge density NIs have been called “superchaotropes” [11,14–16].

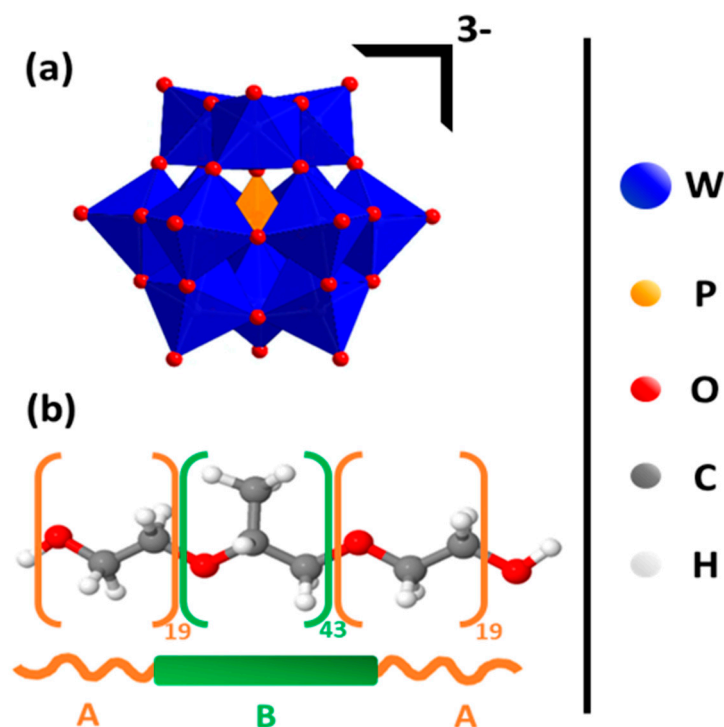


Figure 1. Molecular representation of (a) the α -Keggin-type anion phosphotungstate ($\text{PW}_{12}\text{O}_{40}^{3-}$, PW) and (b) the triblock copolymer P84, providing an ABA architecture (Pluronic[®]-type (BASF, Ludwigshafen, Germany)) with A: ethylene oxide and B: propylene oxide. A sketch of P84 is shown below the molecular structure.

A broad spectrum of nonionic systems was probed regarding their binding with superchaotropic NIs, such as small aromatic molecules [17], surfactant self-assemblies [11,15,18,19], oligo- and polymers [18,20,21], macrocyclic molecules [14,16,22–24] and short-chain amphiphiles [25].

In a previous contribution, our group has explicitly drawn a focus on the interaction of PW with polyethylene oxide (PEO) oligomers. We showed that PW in its acidic form, i.e., $\text{H}_3\text{PW}_{12}\text{O}_{40}$ (HPW), and PEO form nano-assemblies comprising one PW and approximately two PEO oligomers [20]. Such strong binding of POMs on PEO chains was also observed on PEO nonionic surfactant micelles [11]. The binding of NIs to the PEO corona of these PEO surfactant micelles was monitored by the surfactant’s cloud point (CP) evolution which was used as a powerful tool to rank the NIs according to their superchaotropicity [15,19,23]. Later, the interaction of HPW with polypropylene oxide (PPO) based chains was investigated. In the presence of dipropylene oxide *n*-propylether (C_3P_2), HPW forms nano- to mesoscopic self-assemblies in aqueous solution [25].

In conclusion, the interaction of HPW was intensively investigated with (i) polymers, (ii) nonionic surfactant micelles, (iii) PEO-based and (iv) PPO-based compounds. One class of compounds which combines all four features (i–iv) is triblock copolymers with an ABA architecture (A: PEO and B: PPO). ABA triblock copolymers are present as unimers (unaggregated form) at low temperature and as micellar aggregates at elevated temperatures (above their critical micellization temperature (CMT)) in aqueous solution [26–29]. Such well-known polymeric surfactants (Pluronic[®] or Polaxamer[®] (BASF, Ludwigshafen, Germany)) are used in a broad field of applications, as they solubilize oily compounds [26,30], are used as drug delivery systems [31,32] or templates in the synthesis of mesoporous materials [33,34]. Therefore, a controlled manipulation (e.g., controlling physicochemical

solution properties such as the aggregation state or as rheology/viscosity) of polymeric surfactants via the chaotropic effect can be of high interest for a broad field of applications.

The goal of the present work is to gain a deeper knowledge on the interactions between a POM (HPW) and organic molecules of different polarity (hydrophilicity/hydrophobicity) in water. It is well-known that superchaotropic POMs interact with both PEO and PPO chains but we do not know to what extent. Therefore, the underlying question of this work is: Is the interaction of HPW specific to PEO or to PPO chains? In other words: What is the effect of increasing hydrophobicity from PEO to PPO on the binding strength of HPW? To answer this question, we investigated the chaotropic effect of the α -Keggin POM, HPW, on the Pluronic[®] surfactant P84, (EO)₁₉(PO)₄₃(EO)₁₉; see Figure 1b. We monitored the CP of P84 as a function of HPW concentration to investigate the HPW-P84 association in water. At low temperatures (P84 unimers), ¹H-nuclear magnetic resonance (¹H-NMR) was used to probe the local environment of the PPO and PEO blocks. Above the CMT (P84 micelles), scattering techniques, i.e., small angle X-ray and neutron scattering (SAXS and SANS, respectively), were used to investigate shape/charge of the micellar assemblies. HPW was chosen as a model POM as it was shown previously to be the most superchaotropic POM among the well-studied Keggin type POMs. P84 was used because it allows (i) unimers and micelles to be studied in a temperature range between room temperature and 60 °C, and (ii) measurements to be made of a CP and its evolution upon POM addition, which makes it possible to easily evaluate the superchaotropic effect. The obtained experimental results are discussed in the context of the two water mediated driving forces [16]: the chaotropic effect (interaction of POM and P84) and the hydrophobic effect (micellization of P84).

2. Materials and Methods

2.1. Materials

Phosphotungstic acid hydrate (H₃PW₁₂O₄₀ · xH₂O, HPW, M = 2898 g/mol, 99.995% purity) was purchased from Sigma Aldrich (St. Louis, MO, USA). Concentration calculations were done with $x_{\text{HPW}} = 17$ (calculated from TGA measurement). P84 (M = 4200 g/mol) was received as a gift from BASF (Ludwigshafen, Germany) and used as obtained. Milli-Q water was used with a conductivity lower than 10.5 µS/cm and a total organic carbon content of 400 ppb.

2.2. Cloud Point (CP) Measurements/Phase Diagrams

For the phase diagrams, 3 g of binary/ternary mixtures were prepared into screwable tubes from borosilicate glass and the samples were heated in a thermostat (Thermomix_1460, B. Braun AG, Melsungen, Germany) in special tube holders. The thermostat was heated with a rate of 1 °C min^{−1}. The expected precision of the measurements is ±1 °C.

2.3. H-Nuclear Magnetic Resonance (¹H-NMR)

Solution ¹H-NMR spectra were recorded with an Avance300 (Bruker, Billerica, MA, USA) spectrometer using tetramethyl silane as an internal standard. Chemical shifts (δ) are provided in parts per million (ppm) and coupling constants (J) are reported in Hertz (Hz). D₂O was used instead of H₂O.

2.4. Small Angle X-ray Scattering (SAXS)

SAXS measurements, using Mo radiation ($\lambda_{\text{Mo}} = 0.071$ nm), were performed on a bench built by XENOCs (Grenoble, France). The scattered beam was recorded using a large online scanner detector (diameter: 345 mm, from MAR Research, Hamburg, Germany). A large q -range (0.2 to 40 nm^{−1}) was covered with an off-center detection. The collimation was applied using a 12:α multilayer Xenocs mirror (for Mo radiation) coupled to two sets of scatter less FORVIS slits providing a 0.8 mm × 0.8 mm X-ray beam at the sample position. Pre-analysis of data was performed using FIT2D software. For the solutions, 1 mm and 2 mm quartz capillaries were used as sample containers. The samples were thermostated

at given temperatures. The usual corrections for background (empty cell and detector noise) subtractions and intensity normalization using a high density polyethylene film as a standard were applied. The experimental resolution was $\Delta Q/Q = 0.05$. Silver behenate in a sealed capillary was used as the scattering vector calibration standard.

2.5. Small Angle Neutron Scattering (SANS)

All measurements were performed on beamline D33 at the Institut Laue-Langevin (ILL) in Grenoble, France (proposal number 10-168). The applied measurement mode was a monochromatic mode ($\lambda_{\text{neutron}} = 0.6$ nm). Detection was done at 2 m and 5 m. Quartz cuvettes from Hellma (Müllheim, Germany) with thicknesses of 1 mm or 2 mm were used as sample containers. The samples were thermostated at given temperatures. The acquisition times were set to 15 min taking into consideration sample thickness and composition, i.e., the scattering. Water was used as a calibrant in order to obtain absolute intensities. The spectra were treated and normalized using the available software on site. Note, that the presented SANS spectra are subtracted by the signal of D₂O but do contain incoherent scattering. The apparatus was controlled by the NOMAD software and the data treatment was done with the GRASP software on site [35].

2.6. Light Scattering

Samples were measured using a Zetasizer Nano ZS from Malvern Instruments (Malvern, UK). The samples were illuminated with a 632.8 nm laser and detection was done in backscattering position at an angle of 173°. One-centimeter quartz glass cuvettes with a plastic cap served as sample containers. Once set into the measurement chamber the samples were equilibrated for 300 s at the set temperature before the acquisition started. Count rates were collected in triplicates for each sample where one measurement consisted of 10 runs of 10 s each, which would then be automatically averaged.

3. Results and Discussion

3.1. P84: Phase Diagram and Aggregation

We investigated first the binary phase diagram of P84 and water at $c(\text{P84}) \leq 10$ wt%; see Figure 2a. This phase diagram showed three different regions, i.e., a transparent (black star), a blueish (red star) and a turbid phase (green star), see pictures in Figure 2a. For $c(\text{P84}) > 1$ wt%, the phase transitions appeared at rather constant temperatures: 60 ± 4 °C (transparent to blueish) and 74 ± 3 °C (blueish to turbid), respectively. Here, the blueish to turbid phase transition temperature was attributed to the CP [29,36]. For $c(\text{P84}) < 1$ wt%, the two phase transitions were shifted to much higher temperatures by decreasing P84 concentration. In the following, a concentration of P84 of 2.5 wt% (6 mmol L^{-1}) was chosen to ensure (i) low concentration dependence on the phase transitions of P84, and (ii) weak intermicellar interaction that was required for a more convenient fitting and interpretation of the scattering experiments.

The count rate of a 2.5 wt% P84 solution was measured as a function of temperature (along red line in Figure 2a); see Figure 2b. The count rate evolution can be divided in three different temperature regimes, called (I), (II) and (III) hereafter. In regime (I) (20–28 °C), the count rate was low (around 300 kcps), as expected for the scattering of unaggregated P84 unimers. In regime (II) (28–54 °C), the count rate increased strongly upon heating. This increase in the scattered light intensity could be attributed to the formation of spherical micelles above 28 °C, which corresponded to the CMT, as expected from previous works [37]. Above the CMT, the micellar core was formed by the partially dehydrated PPO chains and the micellar corona contained well-hydrated PEO chains [37,38]. At higher temperatures in regime (III), i.e., above 55 °C, a drastic increase in the count rate was observed. This high increase in the scattered intensity was attributed to the formation of rod-like micelles; see Figure 2c. Indeed, this was in agreement with previous works where a transition from spherical to rod-like micelles was reported at 55 °C [38]. The blueish phase obtained in Figure 2a likely arose from elongating rod-like micelles (Tyndall scattering

typically in the (sub-) μm regime). In the present study, the focus was on unimers and spherical micelles. Therefore, we investigated P84 (2.5 wt%) at 20 °C (unimers) and 50 °C (spherical micelles).

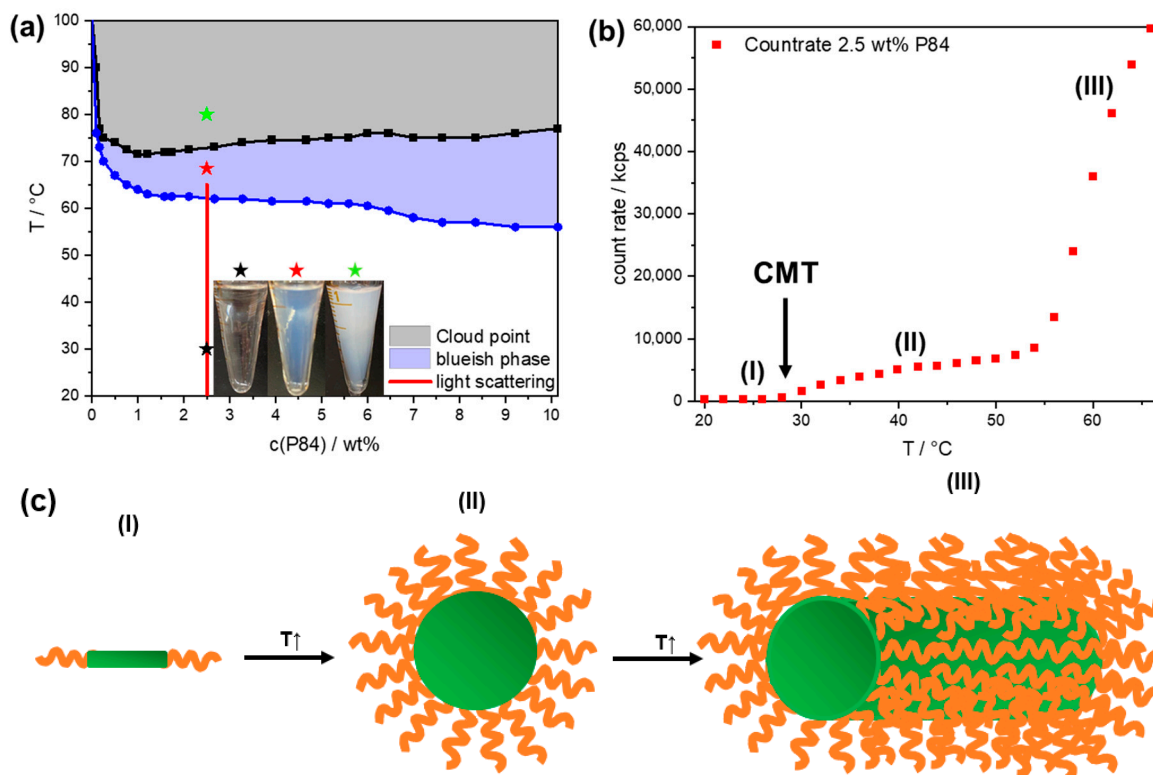


Figure 2. (a) The binary phase diagram of water and P84 up to $c(\text{P84}) = 10 \text{ wt}\%$ shows the presence of a transparent, a blueish and a turbid phase, which is related to the CP of P84. (b) Count rate of 2.5 wt% P84 as a function of temperature; see red line in (a), indicating the presence of three types of aggregation of P84 (I)–(III). (c) Schematic representation of the P84 transition with increasing temperature. At room temperature (I) unimers are present which self-assemble to spherical micelles in (II) and to rod-like micelles in (III). In the following emphasis is put on unimers and spherical micelles.

3.2. P84: Cloud Point Evolution upon Addition of HPW

The CP evolution of a nonionic surfactant upon the addition of POMs was established as a simple but efficient tool to classify the adsorption of NIs on micelles [15]. Hence, the CP and occurrence of the blueish phase at 2.5 wt% P84 was recorded as a function of $c(\text{HPW})$; see Figure 3. In the absence of HPW, the blueish phase occurred at 62 °C and the CP at 72.5 °C. The blueish phase shifted to higher temperatures upon increasing HPW concentration (87 °C for 1 mmol kg^{-1} HPW), while the temperature of the transparent-to-blueish transition increased and then leveled off upon HPW addition. The CP increase was tremendous, as it increased from 72.5 °C up to 100 °C in a very narrow range of concentration (from 0 to $0.05 \text{ mmol kg}^{-1}$ HPW). Such a strong CP increase at low HPW concentration indicated a strong association constant that could be roughly estimated ($K_A \sim 20.0 \text{ mM}^{-1}$; see the fitting results, red curve in Figure 3) from a Langmuir fit according to a previous procedure [15]. The association of HPW with P84 was then around one order of magnitude stronger than with previously investigated systems (using CP measurement to estimate the association constant): poly-N-isopropylamide (PNiPAM10000, $K_A \sim 2.1 \text{ mM}^{-1}$) [21], polyethoxylated micelles (C_8E_4 , $K_A \sim 1.4 \text{ mM}^{-1}$) [15]. This stronger association constant obtained with P84 was likely due to stronger binding to the more hydrophobic (but still hydrated) PPO chains.

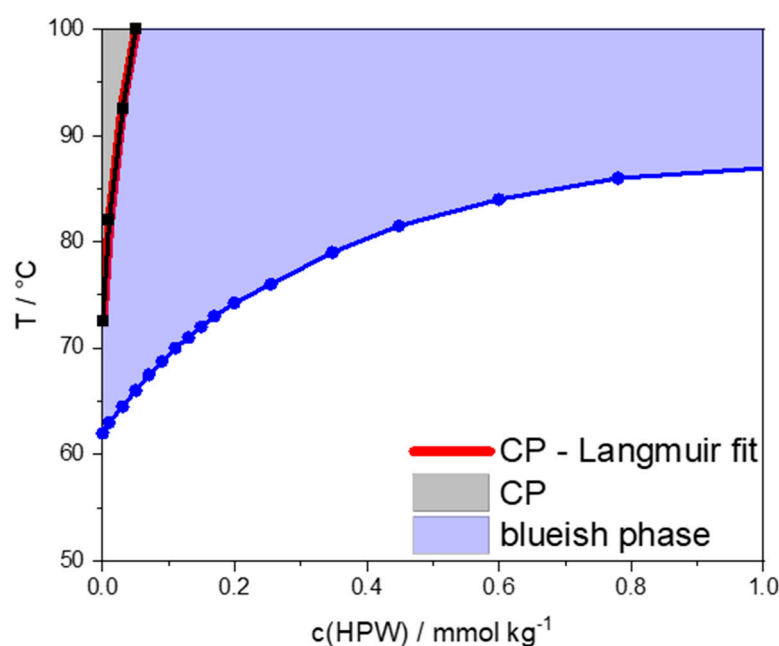


Figure 3. Phase diagram of 2.5 wt% P84 as a function of $c(\text{HPW})$ showing a tremendous CP increase (dark squares) and a strong increase in the temperature of appearance of the blueish phase (blue circles). The red line shows the Langmuir fit of the CP evolution.

Note, that above 6 mmol kg^{-1} HPW, the system phase demixed (precipitation), which likely arose from the strong HPW-P84 binding. The ternary phase diagram water-P84-HPW at room temperature is given in Figure S1.

3.3. Association of HPW with P84 Unimers

To obtain detailed information on the interaction of HPW with P84, unimeric P84 (20°C , 2.5 wt%) was investigated by ^1H -NMR in the presence of HPW.

First, we checked that P84 remains in the unimeric form in the presence of HPW by SANS (Figure S2) and SAXS (Figures S3 and S4); see the corresponding discussion in Section S2.

^1H NMR spectrum for P84 2.5 wt% in D_2O is given in Figure 4b. P84 contains several NMR-active protons: (i) CH_2 protons of the PEO moieties (red ellipse), (ii) the quaternary proton (yellow circle) in PPO, (iii) CH_2 protons (green ellipse) in PPO and (iv) protons in the methyl group (blue ellipse) in PPO; see Figure 4a. These protons were assigned using Shoolery's rules; see Figure 4b, bottom spectrum [39].

- (i) The CH_2 protons of PEO produced a sharp singlet at 3.55 ppm.
- (ii) The quaternary proton of PPO produced a multiplet at around 3.49 ppm as it coupled with all the neighboring CH_2/CH_3 protons in PPO via a ^3J coupling.
- (iii) The CH_2 protons of PPO were detected at around 3.41 ppm as a doublet that was overlaid by the multiplet of the PPO quaternary proton (ii).
- (iv) The CH_3 protons of PPO produced a doublet at 1.01 ppm.

^1H -NMR was measured for 2.5 wt% P84 in the presence of HPW, for $c(\text{HPW}) \leq 5.5 \text{ mmol kg}^{-1}$; see Figures 4b and S5. A broadening of all peaks was observed by increasing HPW concentration. This peak broadening resulted from a decreased diffusion of the P84 molecules in solution, i.e., due to the formation of [HPW-P84] assemblies, as previously observed by investigating the superchaotropic effect of HPW on PEO oligomers [20] and γ -cyclodextrin [23].

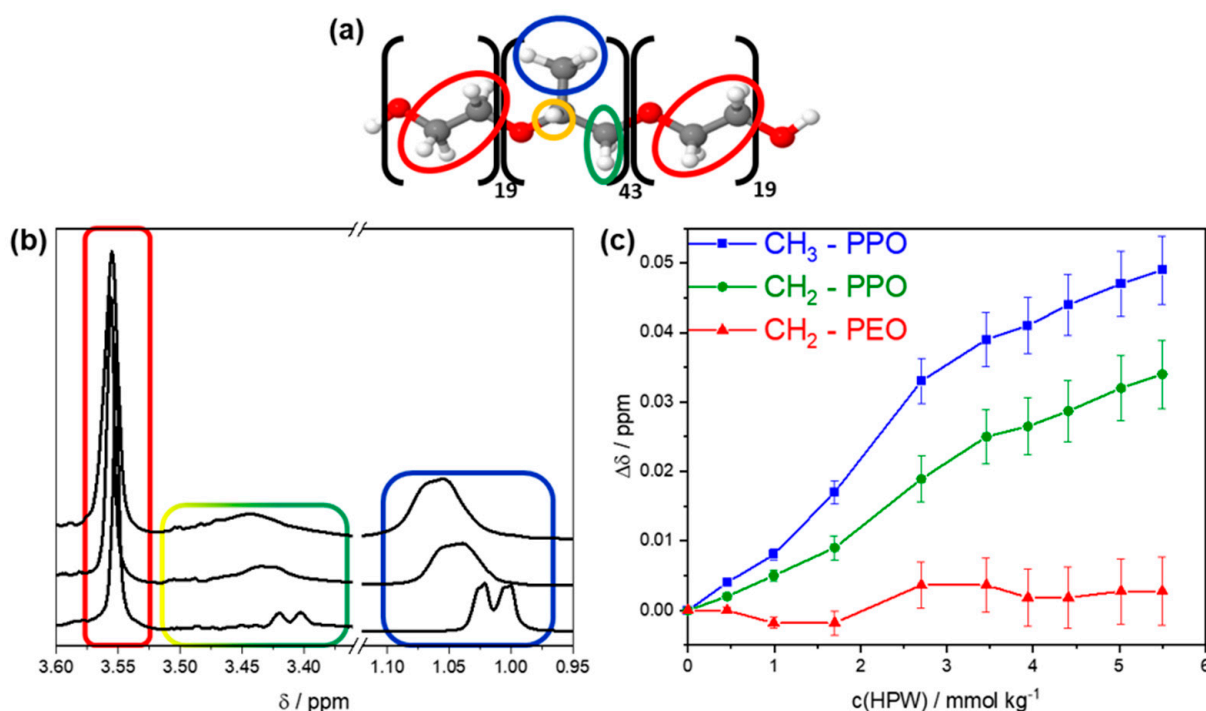


Figure 4. (a) Molecular representation of P84 with ¹H-NMR active protons marked in colored ellipses with following scheme: CH₂ protons of the PEO moieties in red and the CH₃ protons of the methyl group (blue), CH₂ protons (green) and the quaternary proton (yellow) in the PPO moiety. (b) Evolution of the ¹H-NMR spectrum of 2.5 wt% P84 upon an increasing concentration of HPW (0, 2.75 and 5 mmol kg⁻¹ from bottom to top). Spectra measured at 20 °C. The color code corresponds to the colors in (a) and therefore indicates the signals stemming from these specific protons. (c) Shift of the chemical shift, i.e., Δδ, of protons in P84 as a function of c(HPW) indicating a strong interaction of HPW exclusively with the PPO part of P84.

Figure 4c shows the shift of chemical shifts, Δδ, of signals stemming from P84 as a function of c(HPW). The CH₂ protons of PEO moieties (singlet) were unaffected by the addition of HPW. In contrast, the peak positions of CH₂ and CH₃ protons of the PPO moieties were strongly downfield shifted, i.e., shifted to higher chemical shifts (ppm): Δδ of 0.035 ppm and 0.05 ppm respectively for CH₂ and CH₃ protons upon addition of 5.5 mmol kg⁻¹ HPW. Note that Δδ could not be determined for the quaternary proton in PPO due to a strong peak broadening; see Figure S5.

In conclusion, HPW binds to P84 unimers due to its polymeric nature (81 repetition units) via the chaotropic effect. In contrast, monomeric species (e.g., only 1 “repetition” unit) are not expected to associate with a chaotropic anion [40] such as PW. Here, the HPW bound selectively to the PPO moiety over to the PEO moieties of P84 unimers. PPO is more hydrophobic than PEO, and therefore, less or more weakly hydrated. Therefore, the stronger and selective adsorption of HPW to PPO resulted from a combination of chaotropic and hydrophobic effects.

3.4. Association of HPW with P84 Micelles

Figure 5a,b show the SANS and SAXS spectra respectively of 2.5 wt% P84 in water (green rectangles) at 50 °C, i.e., above the CMT. The SANS spectrum of 2.5 wt% P84 in D₂O (green symbols in Figure 5a) shows the typical shape obtained for isotropic scattering objects which can be attributed to P84 micelles. To obtain more information on the micelles, a core (PPO-part)-shell (PEO-part) sphere model was used to fit the experimental data (red line in Figure 5a). The influence of micelle-micelle interactions was considered using a hard-sphere structure factor S(q); see details in Section S4.2 and Table S3.

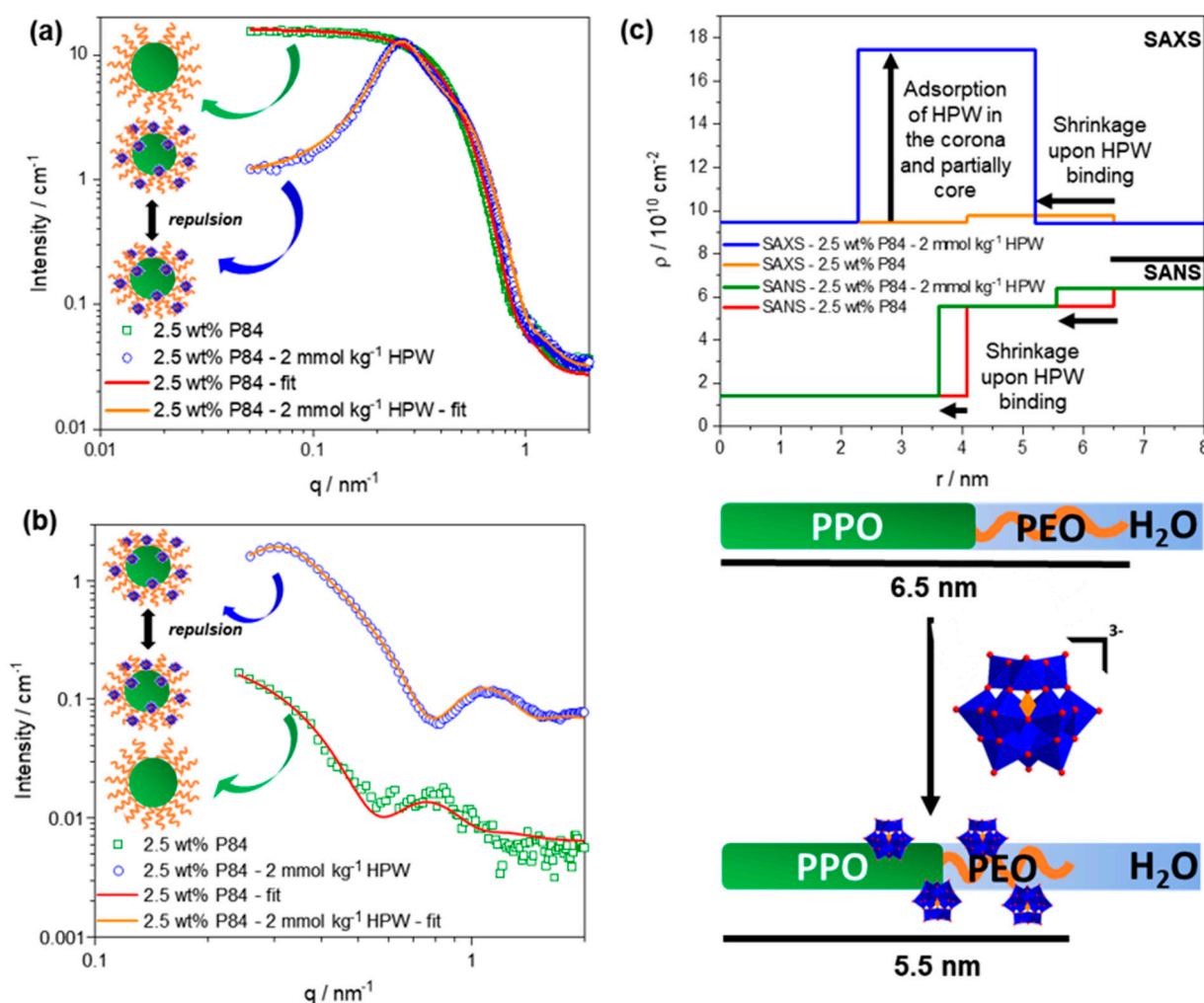


Figure 5. (a) SANS and (b) SAXS spectra of 2.5 wt% P84 in water (D₂O or H₂O respectively) and in the presence of 2 mmol kg⁻¹ HPW at 50 °C including fits. (c) Scattering length density profiles of a P84 micelle in aqueous solution showing that the major contrast giving moiety is PPO in SANS and PEO in SAXS in absence of POM. In presence of HPW, the scattering length density in SAXS is dominated by the PW anions, which are located mostly in the PEO corona. The sketch represents the size shrinkage of P84 micelles and the penetration of PW anions in the micellar PEO corona and partially the micellar PPO core. In the sketch, one P84 represents the whole micelle.

The fit could effectively reproduce the experimental data and revealed a micellar radius of 6.5 nm with a core radius is 4.1 nm (PPO part), a shell thickness (PEO corona) of 2.4 nm and an aggregation number of around 60. These values are in good agreement with those in the literature [29,41], see also Table S2.

In Figure 5b, the SAXS spectrum of 2.5 wt% P84 in H₂O (green rectangles) is presented. The SAXS spectrum differed a lot from that of SANS because of the different scattering length density (ρ) profiles of the micelles in SAXS and SANS; see the orange (SAXS) and red (SANS) curves in Figure 5c. SAXS is mostly sensitive to the (higher electron density) PEO-corona whereas SANS is mostly sensitive to the micellar dehydrated PPO-core [26]. A fit was applied to the SAXS spectrum which perfectly reproduced the experimental spectrum (for details, see Section S4.2 and Table S4). The fitting results were in good agreement with the literature [29].

SANS and SAXS spectra were collected in the presence of HPW (2 mmol kg⁻¹) for 2.5 wt% P84 (blue circles). HPW is “invisible” in SANS, as its scattering length density is close to that of D₂O, whereas it shows a large contrast with H₂O and P84 in SAXS; see Table S1. The SANS spectrum of 2.5 wt% P84—2 mmol kg⁻¹ HPW showed a similar shape

to that of 2.5 wt% P84 for $q > 0.4 \text{ nm}^{-1}$. At $q = 0.26 \text{ nm}^{-1}$, a pronounced correlation peak occurred in the presence of HPW. The correlation peak and the low scattered intensity in the low q ($< 0.26 \text{ nm}^{-1}$) reflected strong repulsive micelle-micelle interactions ($S(q)$). These repulsive interactions upon addition of HPW were attributed to electrostatic repulsions resulting from the adsorption of the negatively charged PWs on the micelles. To obtain more information, the experimental SANS spectrum was fitted by using a core-shell sphere model with a Hayter-MSA $S(q)$ that took into account for electrostatic repulsions [42,43]. The fit reproduced the experimental data perfectly. The result of the fit revealed a micellar radius of 5.5 nm with a micellar core (PPO) radius of 3.6 nm and a shell thickness (PEO) of 1.9 nm (for details, see Section S4.2 and Table S5). Therefore, SANS suggests that upon the addition of HPW, the radius of P84 micelles shrinks from 6.5 nm to 5.5 nm. This effect is reasonable, as PEO is known to “wrap around” PW upon binding [11,20]. The charge of the micelles obtained from the fitting was 47. From the micelle charge, the number of PW anions per micelle was estimated at around 16, i.e., $47/3$, if full dissociation of HPW was considered.

The SAXS spectrum of 2.5 wt% P84—2 mmol kg^{-1} HPW (blue circles in Figure 5b) differed greatly from that of SAXS of 2.5 wt% P84 (green squares in Figure 5b): (i) the overall scattered intensity was strongly increased (by a factor of ten), (ii) a correlation peak occurred at 0.31 nm^{-1} , (iii) an oscillation appeared at 1.12 nm^{-1} and (iv) the scattered intensity decreased at $q < 0.31 \text{ nm}^{-1}$. The overall intensity increase was attributed to the adsorption of the high electron density (ρ^{SAXS}) HPW. The location of the correlation peak and the pronounced oscillation could only be explained by a tremendous change of the scattering length density profile of P84 micelles. The decreased scattered intensity in the low q -regime resulted from the adsorption of charged PW anions on the micelles that induced strong electrostatic repulsions between the micelles, as observed in the SANS spectrum (see Figure 5a, blue circles). Therefore, a core-shell model with a Hayter-MSA $S(q)$ was used to fit the experimental data. The fit yielded a micellar core radius of 2.3 nm, composed of PPO, and a shell thickness 2.9 nm, composed partly of the PPO chains and of the PEO chains with adsorbed HPW (see Section S4.2 and Table S6). HPW was mostly located in the well-hydrated PEO chains and only partly in the dehydrated PPO micellar core close the PEO-PPO region (as in the sketch in the lower part of Figure 5c). These results were confirmed by evaluating the effect of each parameter in the fit; see Section S4.2, Figure S6 and Table S7.

The SAXS/SANS fitting results are summarized in Figure 5c, which shows the ρ profiles in 1D along the micelle (i.e., from its center to the surrounding water) in SANS (green and red curves) and SAXS (blue and orange curves) of P84 micelles in presence (green and blue curves) and absence (red and orange curves) of HPW. r is the distance from the center of the micelle to the surrounding (heavy) water. In SANS for P84 micelles in D_2O (green line in Figure 5c), ρ of the PPO micellar core and of the PEO corona were fitted ($\rho_{\text{PPO}}^{\text{SANS}} = 1.40 \cdot 10^{10} \text{ cm}^{-2}$ and $\rho_{\text{PEO}}^{\text{SANS}} = 5.55 \cdot 10^{10} \text{ cm}^{-2}$) and the values were found to be in agreement with those in the literature [26]. $\rho_{\text{D}_2\text{O}}^{\text{SANS}}$ for the solvent was fixed to $6.40 \cdot 10^{10} \text{ cm}^{-2}$. Upon addition of HPW, the ρ profiles clearly indicated micelle shrinkage (from green to red curve in Figure 5c). In SAXS for P84 micelles in H_2O (orange line in Figure 5c) the major contrast is produced between the PEO ($\rho_{\text{PEO}}^{\text{SAXS}} = 9.75 \cdot 10^{10} \text{ cm}^{-2}$) and PPO/ H_2O ($\rho_{\text{PPO}}^{\text{SAXS}} = 9.47 \cdot 10^{10} \text{ cm}^{-2} \approx \rho_{\text{H}_2\text{O}}^{\text{SAXS}} = 9.40 \cdot 10^{10} \text{ cm}^{-2}$). Upon the addition of HPW, the ρ^{SAXS} profile drastically changed (from the orange to the blue curve in Figure 5c). A strong increase in ρ , i.e., up to $18.70 \cdot 10^{10} \text{ cm}^{-2}$, was obtained for $2.3 \leq r \leq 5.1 \text{ nm}$, which could only be attributed to the presence of PW.

We concluded by combining SAXS and SANS results that (i) the addition of HPW to P84 micelles led to a size decrease of P84 micelles, and (ii) HPW mostly adsorbs on the PEO micelle corona; see sketch in Figure 5c.

4. Conclusions

In the first part, we investigated the different aggregation states of the polymeric P84 (ABA block copolymer) surfactant in aqueous solution. At 2.5 wt%, unimers of P84 were present at 20 °C. By increasing temperature above the CMT (28 °C), spherical micelles were observed at 50 °C. The micelles underwent a sphere-to-rod transition at >55 °C. The tremendous CP increase of 2.5 wt% P84 in the presence of micromolar concentrations of HPW confirmed the strong association between HPW and P84, with an adsorption constant of $K_A \sim 20.0 \text{ mM}^{-1}$. Interestingly, such a high K_A was never observed for the binding of HPW with other polymers (PNiPAM) or micelles (C_8E_4).

It was shown by ^1H -NMR experiments that HPW selectively binds to the PPO moiety of P84 unimers (below the CMT at 20 °C). This effect was attributed to a combination of the chaotropic and hydrophobic effects due to the higher hydrophobicity of PPO over PEO.

Via the combination of SANS/SAXS and modeling, spherical micelles of P84 with a radius of 6.5 nm (4.1 nm PPO core and 2.4 nm PEO corona) were observed in the absence of HPW above the CMT at 50 °C. Upon the addition of HPW, the micelle shrank in size down to a radius of 5.5 nm. HPW were found to be mostly located in the micellar PEO corona and only partially in the PPO micellar core (close the PEO-PPO region). Therefore, upon heating above the CMT, the micellization of P84—driven by the hydrophobic effect—led to the displacement of HPW from PPO to PEO.

This study shines light on the subtle balance of two effects: the chaotropic effect (binding of HPW to P84) and the hydrophobic effect (driving the micellization of P84 and the binding of HPW to P84).

We have shown here that HPW selectively adsorbs on the PPO moieties over the PEO chains; therefore, we could conclude that HPW interacts more strongly with PPO as a result of an increased hydrophobic character compared to PEO. A deeper knowledge of the interactions between a POM and organic molecules in water is a first step toward designing formulations containing POM building blocks showing specific interactions, i.e., toward molecular recognition. This deeper knowledge is required for the future development of POM applications, for instance in the medical field [4], for which pharmaceutical formulations containing POM and organic molecules (such as polymeric additives [44]) could be developed and specific interactions with biological molecules may be required. We can foresee applications of our findings for the control of polymeric surfactants as oil solubilizers or delivery systems, as the binding of POMs is likely to strongly impact the solubilizing efficiency of polymeric surfactant micelles. In conclusion, the balance of the chaotropic and hydrophobic effects may play a decisive role in the assembly of hierarchical functional systems.

Supplementary Materials: The following supporting information can be downloaded at: <https://www.mdpi.com/article/10.3390/colloids6010016/s1>, Figure S1: Partial ternary phase diagram water/P84/HPW provided in weight fraction (xweight) at room temperature. The grey zone shows the biphasic region, whereas the blue area provides phases which appear blueish. The green ellipse indicates the area, in which it was worked in this contribution; Figure S2: SANS spectra of 2.5 wt% P84 in D₂O at 20 °C. The spectra indicate that upon the addition of 2 mmol kg^{−1} HPW no significant aggregation of P84 takes place; Figure S3: (a) SAXS spectra of 2.5wt% P84 in water as a function of temperature between 20 and 60 °C. (b) SAXS spectra of 2.5 wt% P84 in presence of 2 mmol kg^{−1} HPW as a function of temperature between 20 and 60 °C. 2 mmol kg^{−1} HPW in water is given as a reference; Figure S4: Count rate of 2.5 wt% P84 obtained by light scattering as a function of temperature (dark rectangles). In the manuscript the kink at 28 °C was attributed to the CMT, i.e., the critical micellization temperature. The intensity of 2.5 wt% P84 in presence of 2 mmol kg^{−1} HPW obtained by SAXS at $q = 0.3 \text{ nm}^{-1}$ (green data). The kink indicates again the CMT. The red region shows that the CMT is in a similar region in absence and presence of 2 mmol kg^{−1} HPW and significantly the POM does not influence the CMT of P84; Figure S5: ^1H -NMR spectra of 2.5 wt% P84 at 20 °C in D₂O in presence of 0, 0.46, 0.99, 1.70, 2.70, 3.46, 3.94, 4.41, 5.02, 5.50 mmol kg^{−1} HPW (bottom to top). The presence of HPW causes a strong shift of signals stemming from the PPO, whereas the PEO signal remains untouched.; Figure S6: Fits obtained with the fitting parameters in

Table S7. While fits (i–iv) do not lead to proper fitting results of the experimental data, fit (v) (POM in PEO corona, penetrating the PPO core) leads to a perfect fit of the experimental data.; Table S1: (Reported) scattering length densities in SAXS and SANS of the investigated compounds. Note, that in case of $\rho(\text{P84})$ the pure PO and EO moiety is taken into account, i.e., hydration water is neglected, while it is known that hydration water increases the scattering length density.; Table S2: Dimension (in nm) of a spherical P84 micelle at $c(\text{P84}) = 5 \text{ wt\%}$.; Table S3: Fitting parameters of 2.5 wt% P84 - SANS - Hard sphere $S(q)$.; Table S4: Fitting parameters of 2.5 wt% P84 - SAXS - Hard sphere $S(q)$.; Table S5: Fitting parameters of 2.5 wt% P84-2 mmol kg^{-1} HPW - SANS - Hayter-MSA $S(q)$.; Table S6: Fitting parameters of 2.5 wt% P84-2 mmol kg^{-1} HPW - SAXS - Hayter-MSA $S(q)$.; Table S7: In- and output fitting parameters of the different fit procedures (i–v). The parameters (i–iv) do not lead to satisfying fits (indicated by the red background colour), whereas parameters in (v) produce a fit, which perfectly describes the measured spectrum (indicated with green background colour), cf. Figure S6.

Author Contributions: Conceptualization: P.S., O.D., P.B. (Pratap Bahadur) and P.B. (Pierre Bauduin); methodology: P.S., X.G., I.G. and P.B. (Pierre Bauduin); software: P.S., I.G., O.D., A.P. and P.B. (Pierre Bauduin); validation: P.S. and P.B. (Pierre Bauduin); formal analysis: P.S. and P.B. (Pierre Bauduin); investigation, P.S. and X.G.; resources: P.B. (Pratap Bahadur), O.D. and A.P.; data curation: P.S. and P.B. (Pierre Bauduin); writing—original draft preparation: P.S.; writing—review and editing: P.S. and P.B. (Pierre Bauduin); visualization: P.S.; supervision: A.P., P.B. (Pierre Bauduin); project administration, O.D., A.P. and P.B. (Pierre Bauduin); funding acquisition: O.D., A.P. and P.B. (Pierre Bauduin). All authors have read and agreed to the published version of the manuscript.

Funding: This research received no external funding.

Institutional Review Board Statement: Not applicable.

Informed Consent Statement: Not applicable.

Data Availability Statement: Data is contained within the article or Supplementary Materials.

Conflicts of Interest: The authors declare no conflict of interest.

References

- Bernardini, G.; Wedd, A.G.; Zhao, C.; Bond, A.M. Photochemical oxidation of water and reduction of polyoxometalate anions at interfaces of water with ionic liquids or diethylether. *Proc. Natl. Acad. Sci. USA* **2012**, *109*, 11552–11557. [[CrossRef](#)] [[PubMed](#)]
- Wang, S.S.; Yang, G.Y. Recent advances in polyoxometalate-catalyzed reactions. *Chem. Rev.* **2015**, *115*, 4893–4962. [[CrossRef](#)] [[PubMed](#)]
- Krickl, S.; Buchecker, T.; Meyer, A.U.; Grillo, I.; Touraud, D.; Bauduin, P.; König, B.; Pfitzner, A.; Kunz, W. A systematic study of the influence of mesoscale structuring on the kinetics of a chemical reaction. *Phys. Chem. Chem. Phys.* **2017**, *19*, 23773–23780. [[CrossRef](#)] [[PubMed](#)]
- Rhule, J.T.; Hill, C.L.; Judd, D.A.; Schinazi, R.F. Polyoxometalates in medicine. *Chem. Rev.* **1998**, *98*, 327–357. [[CrossRef](#)]
- Fukuma, M.; Seto, Y.; Yamase, T. In vitro antiviral activity of polyoxotungstate (PM-19) and other polyoxometalates against herpes simplex virus. *Antivir. Res.* **1991**, *16*, 327–339. [[CrossRef](#)]
- Stephan, H.; Kubeil, M.; Emmerling, F.; Müller, C.E. Polyoxometalates as versatile enzyme inhibitors. *Eur. J. Inorg. Chem.* **2013**, *2013*, 1585–1594. [[CrossRef](#)]
- Yamase, T. Photo- and electrochromism of polyoxometalates and related materials. *Chem. Rev.* **1998**, *98*, 307–326. [[CrossRef](#)]
- Bijelic, A.; Rempel, A. The use of polyoxometalates in protein crystallography—An attempt to widen a well-known bottleneck. *Coord. Chem. Rev.* **2015**, *299*, 22–38. [[CrossRef](#)]
- Misra, A.; Kozma, K.; Streb, C.; Nyman, M. Beyond charge balance: Counter-cations in polyoxometalate chemistry. *Angew. Chem. Int. Ed.* **2019**, *59*, 596–612. [[CrossRef](#)]
- Bera, M.K.; Qiao, B.; Seifert, S.; Burton-Pye, B.P.; Olvera De La Cruz, M.; Antonio, M.R. Aggregation of heteropolyanions in aqueous solutions exhibiting short-range attractions and long-range repulsions. *J. Phys. Chem. C* **2016**, *120*, 1317–1327. [[CrossRef](#)]
- Naskar, B.; Diat, O.; Nardello-Rataj, V.; Bauduin, P. Nanometer-size polyoxometalate anions adsorb strongly on neutral soft surfaces. *J. Phys. Chem. C* **2015**, *119*, 20985–20992. [[CrossRef](#)]
- Hofmeister, F. Zur Lehre von der Wirkung der Salze. *Arch. Exp. Pathol. Pharmacol.* **1888**, *25*, 1–30. [[CrossRef](#)]
- Kunz, W.; Henle, J.; Ninham, B.W. “Zur Lehre von der Wirkung der Salze” (about the science of the effect of salts): Franz Hofmeister’s historical papers. *Curr. Opin. Colloid Interface Sci.* **2004**, *9*, 19–37. [[CrossRef](#)]
- Assaf, K.I.; Ural, M.S.; Pan, F.; Georgiev, T.; Simova, S.; Rissanen, K.; Gabel, D.; Nau, W.M. Water structure recovery in chaotropic anion recognition: High-affinity binding of dodecaborate clusters to γ -cyclodextrin. *Angew. Chem. Int. Ed.* **2015**, *54*, 6852–6856. [[CrossRef](#)]

15. Buchecker, T.; Schmid, P.; Renaudineau, S.; Diat, O.; Proust, A.; Pfitzner, A.; Bauduin, P. Polyoxometalates in the Hofmeister series. *Chem. Commun.* **2018**, *54*, 1833–1836. [[CrossRef](#)] [[PubMed](#)]
16. Assaf, K.I.; Nau, W.M. The chaotropic effect as an assembly motif in chemistry. *Angew. Chem. Int. Ed.* **2018**, *57*, 13968–13981. [[CrossRef](#)] [[PubMed](#)]
17. Qi, B.; An, S.; Luo, J.; Liu, T.; Song, Y.-F. Enhanced macroanion recognition of superchaotropic kegglin clusters achieved by synergy of anion– π and anion–cation interactions. *Chem. A Eur. J.* **2020**, *26*, 16802–16810. [[CrossRef](#)] [[PubMed](#)]
18. Merhi, A.T.; Jonchère, A.; Girard, L.; Diat, O.; Nuez, M.; Viñas, C.; Bauduin, P. Highlights on the Binding of Cobalt-Bis-(Dicarbollide) with Glucose Units. *Chem. A Eur. J.* **2020**, *26*, 13935–13947. [[CrossRef](#)]
19. Hohenschutz, M.; Grillo, I.; Diat, O.; Bauduin, P. How nano-ions act like ionic surfactants. *Angew. Chem. Int. Ed.* **2020**, *59*, 8084–8088. [[CrossRef](#)]
20. Buchecker, T.; LeGoff, X.; Naskar, B.; Pfitzner, A.; Diat, O.; Bauduin, P. Polyoxometalate/polyethylene glycol interactions in water: From nano-assemblies in water to crystal formation by electrostatic screening. *Chem. A Eur. J.* **2017**, *23*, 8434–8442. [[CrossRef](#)]
21. Buchecker, T.; Schmid, P.; Grillo, I.; Prévost, S.; Drechsler, M.; Diat, O.; Pfitzner, A.; Bauduin, P. Self-assembly of short chain Poly-N-isopropylacrylamid (PNIPAM) induced by superchaotropic Keggin Polyoxometalates: From globules to sheets. *J. Am. Chem. Soc.* **2019**, *141*, 6890–6899. [[CrossRef](#)]
22. Falaise, C.; Moussawi, M.A.; Floquet, S.; Abramov, P.A.; Sokolov, M.N.; Haouas, M.; Cadot, E. Probing dynamic library of metal-oxo building blocks with γ -cyclodextrin. *J. Am. Chem. Soc.* **2018**, *140*, 11198–11201. [[CrossRef](#)] [[PubMed](#)]
23. Yao, S.; Falaise, C.; Ivanov, A.A.; Leclerc, N.; Hohenschutz, M.; Haouas, M.; Landy, D.; Shestopalov, M.A.; Bauduin, P.; Cadot, E. Hofmeister effect in the Keggin-type polyoxotungstate series. *Inorg. Chem. Front.* **2021**, *8*, 12–25. [[CrossRef](#)]
24. Assaf, K.I.; Begaj, B.; Frank, A.; Nilam, M.; Mougharbel, A.S.; Kortz, U.; Nekvinda, J.; Grüner, B.; Gabel, D.; Nau, W.M. High-affinity binding of metallacarborane cobalt bis(dicarbollide) anions to cyclodextrins and application to membrane translocation. *J. Org. Chem.* **2019**, *84*, 11790–11798. [[CrossRef](#)] [[PubMed](#)]
25. Schmid, P.; Buchecker, T.; Khoshima, A.; Touraud, D.; Diat, O.; Kunz, W.; Pfitzner, A.; Bauduin, P. Self-assembly of a short amphiphile in water controlled by superchaotropic Polyoxometalates: $H_4SiW_{12}O_{40}$ vs. $H_3PW_{12}O_{40}$. *J. Coll. Interface Sci.* **2021**, *587*, 347–357. [[CrossRef](#)]
26. Grillo, I.; Morfin, I.; Prévost, S. Structural characterization of pluronic micelles swollen with perfume molecules. *Langmuir* **2018**, *34*, 13395–13408. [[CrossRef](#)]
27. Štuncová, A.; Schmidt, P.; Dybal, J. Role of hydration and water coordination in micellization of Pluronic block copolymers. *J. Colloid Interface Sci.* **2010**, *352*, 415–423. [[CrossRef](#)]
28. Álvarez-Ramírez, J.G.; Fernández, V.V.A.; Macías, E.R.; Rharbi, Y.; Taboada, P.; Gámez-Corrales, R.; Puig, J.E.; Soltero, J.F.A. Phase behavior of the Pluronic P103/water system in the dilute and semi-dilute regimes. *J. Coll. Interface Sci.* **2009**, *333*, 655–662. [[CrossRef](#)]
29. Jain, N.J.; Aswal, V.K.; Goyal, P.S.; Bahadur, P. Salt induced micellization and micelle structures of PEO/PPO/PEO block copolymers in aqueous solution. *Colloids Surf. A* **2000**, *173*, 85–94. [[CrossRef](#)]
30. Liu, H.-Y.; Prévost, S.; Gradzielski, M. Solubilisation of oils of different polarity in aqueous solutions of pluronic triblock copolymers. *Z. Phys. Chem.* **2012**, *226*, 675–694. [[CrossRef](#)]
31. Bodratti, A.M.; Alexandridis, P. Formulation of poloxamers for drug delivery. *J. Funct. Biomater.* **2018**, *9*, 11. [[CrossRef](#)] [[PubMed](#)]
32. Batrakova, E.V.; Kabanov, A.V. Pluronic block copolymers: Evolution of drug delivery concept from inert nanocarriers to biological response modifiers. *J. Control. Release* **2008**, *130*, 98–106. [[CrossRef](#)]
33. Yue, M.B.; Chun, Y.; Cao, Y.; Dong, X.; Zhu, J.H. CO_2 capture by as-prepared SBA-15 with an occluded organic template. *Adv. Funct. Mater.* **2006**, *16*, 1717–1722. [[CrossRef](#)]
34. Bronich, T.K.; Bontha, S.; Shlyakhtenko, L.S.; Bromberg, L.E.; Hatton, V.; Kabanov, T.A.A.V. Template-assisted synthesis of nanogels from Pluronic-modified poly (acrylic acid). *J. Drug Target* **2006**, *14*, 357–366. [[CrossRef](#)]
35. Dewhurst, C.D.; Grillo, I.; Honecker, D.; Bonnaud, M.; Jacques, M.; Amrouni, C.; Perillo-Marcone, A.; Manzin, G.; Cubitt, R. The small-angle neutron scattering instrument D33 at the Institut Laue–Langevin. *J. Appl. Crystallogr.* **2016**, *49*, 1–14. [[CrossRef](#)]
36. Patel, T.; Bahadur, P.; Mata, J. The clouding behaviour of PEO-PPO based triblock copolymers in aqueous ionic surfactant solutions: A new approach for cloud point measurements. *J. Colloid Interface Sci.* **2010**, *345*, 346–350. [[CrossRef](#)] [[PubMed](#)]
37. Alexandridis, P.; Holzwarth, J.F.; Hatton, T.A. Micellization of poly(ethylene oxide)-poly(propylene oxide)-poly(ethylene oxide) triblock copolymers in aqueous solutions: Thermodynamics of copolymers association. *Macromolecules* **1994**, *27*, 2414–2425. [[CrossRef](#)]
38. Khimani, M.; Rao, U.; Bahadur, P.; Bahadur, P. Calorimetric and scattering studies on micellization of pluronics in aqueous solutions: Effect of the size of hydrophilic PEO end blocks, temperature, and added salt. *J. Dispers. Sci. Technol.* **2014**, *35*, 1599–1610. [[CrossRef](#)]
39. Mohan, J. *Organic Spectroscopy: Principles and Applications*, 2nd ed.; Alpha Science: Paris, France, 2004.
40. Rogers, B.A.; Okur, H.I.; Yan, C.; Yang, T.; Heyda, J.; Cremer, P.S. Weakly hydrated anions bind to polymers but not monomers in aqueous solutions. *Nat. Chem.* **2022**, *14*, 40–45. [[CrossRef](#)]
41. Liu, Y.; Chen, S.; Huang, J.S. Small-Angle Neutron Scattering Analysis of the Structure and Interaction of Triblock Copolymer Micelles in Aqueous Solution. *Macromolecules* **1998**, *31*, 2236–2244. [[CrossRef](#)]
42. Hayter, J.B.; Penfold, J. An analytic structure factor for macroion solutions. *Mol. Phys.* **1981**, *42*, 109–118. [[CrossRef](#)]

-
43. Hansen, J.; Hayter, J.B. A rescaled MSA structure factor for dilute charged colloidal dispersions. *Mol. Phys.* **1982**, *46*, 651–656. [[CrossRef](#)]
 44. Pitto-Barry, A.; Barry, N.P.E. Pluronic block-copolymers in medicine: From chemical and biological versatility to rationalisation and clinical advances. *Polym. Chem.* **2014**, *5*, 3291–3297. [[CrossRef](#)]